Turkish Journal of Electrical Engineering & Computer Sciences

http://journals.tubitak.gov.tr/elektrik/

Research Article

Turk J Elec Eng & Comp Sci
(2021) 29: 2346 – 2361

doi:10.3906/elk-2012-68

A 1-kW wireless power transfer system for electric vehicle charging with hexagonal flat spiral coil

Emrullah AYDIN[1,2,*], **M. Timur AYDEMİR**[2,3]

[1]Department of Electrical-Electronic Engineering , Faculty of Engineering and Natural Sciences, Malatya Turgut Özal University, Malatya, Turkey

[2]Department of Electrical-Electronic Engineering , Faculty of Engineering, Gazi University, Ankara, Turkey

[3]Department of Electrical-Electronic Engineering , Faculty of Engineering and Natural Sciences, Kadir Has University, İstanbul, Turkey

Received: 13.12.2020 • **Accepted/Published Online:** 22.03.2021 • **Final Version:** 23.09.2021

Abstract: Wireless power transfer (WPT) technology is getting more attention in these days as a clean, safe, and easy alternative to charging batteries in several power levels. Different coil types and system structures have been proposed in the literature. Hexagonal coils, which have a common usage for low power applications, have not been well studied for high and mid power applications such as in electric vehicle (EV) battery charging. In order to fill this knowledge gap, the self and mutual inductance equations of a hexagonal coil are obtained, and these equations have been used to design a 1 kW WPT system with hexagonal coils for a mid-power stage EV charging. The theoretical and simulation results have been validated with an implementation in the laboratory and a DC-to-DC power efficiency of 85% is achieved across a 10 cm air gap between the perfect aligned coils. The misalignment performance of the system was observed for different positioning of the secondary coil, and the output power variation is given. In addition, the effect of shielding on magnetic field exposition of a driver sitting in an EV was obtained, and these simulation results were compared in order to check the compliance with international health standards.

Key words: Wireless power transfer (WPT), inductive power transfer, inductance calculation, electric vehicles (EVs)

1. Introduction

The use of batteries has been rapidly becoming widespread in many areas, from small to high power applications, in order to reduce the limitations of movement caused by the use power connections. The increase in battery usage has raised the problem of how to charge these batteries more easily and efficiently. wireless power transfer (WPT) systems for battery charging have recently become of interest as they offer ease of use, high safety, high reliability, low maintenance costs and long service life. Due to these advantages, they have a wide range of use in mobile phones, electric vehicles, biomedical implants, space applications, textile applications, and military field applications [1–7]. Since the first idea of transferring power wirelessly was introduced by Nikola Tesla in 1890, many important developments have taken place in this field. In the first years, power transfers were realized with low efficiency from small air gaps (mm). In addition, the use of massive ferrite bars for directing the flux and obtaining high coupling coefficients was quite common. One of the first known examples of the wireless charging of electric vehicles is described in the patent issued to researchers Hutin and Le-Blanc [8]. There was not much development in this area until the early 1980s. In 1984, a long ferrite bar was used to transfer power

*Correspondence: emrullah.aydin@ozal.edu.tr

between the primary and secondary coils at a distance of only a few mm [9]. In another study, it was aimed to reduce the switching losses by connecting parallel capacitors to the thyristors to get a high-efficiency wireless power transfer system [10]. In the early 2000s, a project was carried out in Genoa, Italy, where buses could be charged wirelessly at the bus stations. In 2007, a group of researchers at MIT succeeded in lighting a 60 W bulb from a distance of about 2.4 m by two self-resonant coils in a strongly coupled regime [11]. This work triggered the interest of scientists around the world. There has been a growing interest now towards WPT systems and their applications to battery charging solutions especially for electric vehicles and consumer electronics.

For the EV applications of the WPT the primary coil is mounted on the ground and the secondary coil is placed under the chassis of the vehicle. The distance between these coils, the transferring power and the operating frequency may be different depending on the type of applications. It is desired to establish a specific power rating standard for EVs, such as 3.7 kW for electric cars and 22 kW for electric buses. But lower power values are preferable for such as electric bicycles and electric golf carts. Larger sized coils, multi-coil designs and optimized mass ferrite cores are some of the solutions proposed for larger air-gap systems. Another problem is misalignment between the coils. Especially for the stationary charging, the alignment between the primary and secondary coils depends on the driver expertise and the parking skills. A comprehensive work is given on stationary charging of EV's and design criteria [12]. In conventional two coil systems the coupling between the coils varies between 0.1 to 0.3. To overcome misalignment problems and allow transferring power to longer distances different coil designs have been proposed. One of the proposed structures is the DDQ coil structure. Two coils are placed in DD type to increase the main flux path to get more efficiency at longer distance between the primary and secondary coils. Also, a quadrature (Q) coil is added to the design to increase the lateral misalignment tolerance of the system [13]. In recent studies another proposed coil type is using multiple coils. either on both sides or only at one side. Adding one or more coil to main coils which are self-resonated increases not only the generated flux but also the apparent coupling coefficient [14–16]. Another study is the dimensioning of the DD coil structure from 300 mm to 1000 mm in order to provide a wide power range, which can be used in all SUVs and sedan type electric vehicles charging [17]. Reducing the leakage flux boosts the flux captured by secondary coil, increasing the coupling between the coils. In order to reduce the leakage flux in DD coil structure, massive ferrite bars are placed at the end corners and leakage flux is reduced by 46% [18]. Another novel coil structure proposed is QDQ (Quad D Quadrature), which has better misalignment tolerance with four small coils placed inside a larger primary coil [19]. A comparison of most used multi-coil structures is given in [20]. According to this comparison results, triangular DQ pad (TDQP) is not preferable since it has a strong magnetic coupling between each part of primary. Bi-polar pad (BPP) has better performance than the rectangular quadrupole pad (RQP) and TDQP. In another study, it was aimed to increase the alignment tolerance with the coil design on both the primary and secondary sides of the cross shape of two rectangles. It has been shown that this design has less sensitivity and a higher coupling coefficient than circular and square coil shapes with low self-inductance values [21]. A multi-sub coil design proposed for a flux pipe type design in [22]. The experimental and simulation results show that the proposed design has a high coupling coefficient since the sub-coils are distributing the magnetic flux density inside the ferrite bars with lowering the peak value of the flux density. A ferrite-less DD coil is proposed by using a reflection coil to decrease the total mess and cost [23]. Besides these novel coil designs, another coil structure is hexagonal coil which comes with some of advantages such as less sensitive to misalignment, more coupling coefficient than the same sized rectangular coil and easy and cost effective to implement multi array coils [24, 25]. When the circular coil, which is the most used coil structure, is used in array coil systems, the number of coils that can be placed in a certain area is low.

In honeycomb coil structure, space can be used efficiently and it provides great advantages especially for the misalignment conditions. This coil structure is generally used for low power with multi-array coil designs. There are limited literatures for high power applications of WPT systems by using hexagonal coil and its inductance calculations. As this knowledge gap is filled, this paper proposes a design with a hexagonal coil for charging electric vehicles.

It is aimed to reduce the total reactive power drawn by adding suitable resonance capacitors to the coils on the primary and / or secondary sides in order to produce a sufficient magnetic field in WPT systems. Basically, while the purpose of compensation on the primary side is to reduce the apparent power at the input, the maximum power transfer is achieved by eliminating the secondary inductance by the compensation capacitor added to the secondary side. The selection of the appropriate compensation topology depends on the requirements of the application. There are four basic topologies: series-series(S-S), series-parallel (S-P), parallel-series (P-S) and parallel-parallel (P-P). Also, there are hybrid compensation topologies that can be used for appropriate applications. The system size increases with the use of compensation circuits. In order to reduce the size and create a more compact structure, a new bipolar coupling structure is proposed by placing the compensation inductance in the center of the main windings [26]. In a series compensated secondary system, the reflected impedance from the secondary does not have any reactive part. For the compensation of the primary side, the use of parallel capacitors is extremely rare due to disadvantages such as large input impedance, complex sets of equations, and dependence on load and coupling coefficient. The resonance frequency of the primary side will be shifted by depending on the variation of mutual inductance in SP and PP compensation topologies. It has been shown that the SS topology requires less copper use compared to the other basic topologies SS topology, with independency of the compensation capacitors on the magnetic coupling and load resonance frequency, has more misalignment tolerance [27–30]. Because of these advantages, SS topology is selected for this work.

An optimization algorithm is proposed for the whole WPT system design for EV applications to determine the optimum number of turns, operating frequency, and wire sections [30]. The Neumann's expression was used to calculate inductance values for the rectangular coil design in the optimization algorithm. This study shows that the self and mutual inductance calculations are an important issue in the design procedure to transfer the desired power to the load. For EV applications the coil sizes are quite large and the calculation of inductance values with finite element analysis (FEA) needs long solution times. Therefore, several methods have been proposed in the literature to calculate the self and mutual inductances for different types of coil sizes and structures. In a recent work, multi-coil designs are well studied in order to increase magnetic coupling of WPT systems and inductance values are obtained by using the Grover's formula [31]. Some of them have accurate results [32, 33]. However, the equations include many coefficients and complex integral forms [34].In this paper, a calculation method based on the Biot Savart law has been used to obtain the self and mutual inductances of hexagonal coils. It has been shown in the literature that higher efficiency systems can be realized by using cores and multiple coil designs [13, 35]. However, the efficiencies obtained in coreless systems consisting of a single primary and secondary are similar to the study obtained in this study. This study supports the idea that the use of hexagonal coil structure is possible in high power applications and aims to show that its use will be advantageous especially in multi-coil array designs. In this paper a 1 kW WPT system for an EV battery charging system with hexagonal coils is proposed and the experimental results obtained from the laboratory tests performed on the prototype system are presented. This proposed charging system can be used for different EVs such as electric bicycles and electric golf carts. The fundamentals of the WPT system are described in the second section. In the third section, the inductance calculation approach and the coil specifications for the hexagonal

coil are given. In the fourth part, simulation of ANSYS Maxwell and Simplorer results are given. In the last part of this study implementation of the system is done and the results are given. In addition, the simulation results of magnetic flux density values exposed by a driver sitting in an electric vehicle were compared with the values allowed by the ICNIRP (International Commission on Non-Ionising Radiation Protection) standard [36] to check compliance with international health standards.

2. Fundamental of WPT systems

Operation of WPT systems are based on the same principles as those of transformers. In the conventional transformers there is a ferrite core and the primary and secondary coils are wound around this core. However, WPT systems have a large air-gap air core transformer with an appropriate compensation topology. The system basically consists of two coils which are magnetically coupled. Figure 1 shows a magnetically coupled WPT system with an S-S compensation topology.

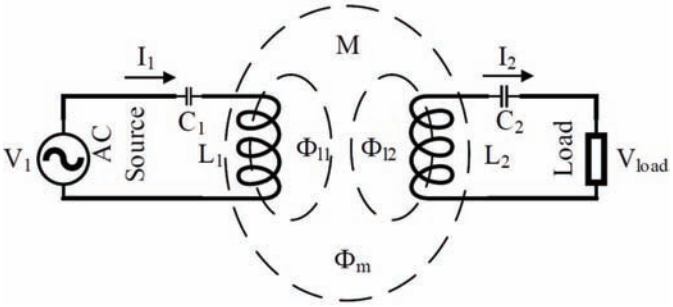

Figure 1. Fundamental structure of S-S compensated WPT.

In Figure 1, $_1$ and $_2$ are the primary and the secondary coils, $\mathbb{C}_1$ and $\mathbb{C}_2$ are the compensation capacitors. M shows the mutual inductance and ϕ_{11} and ϕ_{12} are the leakage flux for the primary and secondary sides, respectively. Coupling coefficient *(k)* and output power equations are given below [37].

$$k = \frac{M}{\sqrt{L_1 L_2}} \tag{1}$$

$$P_{out} = \frac{\omega_0 I_1^2 M^2 Q_2}{L_2} = \omega_0 L_1 I_1^2 k^2 Q_2 \tag{2}$$

where ω_0 is the resonant frequency and $\mathbb{Q}_2$ is the quality factor of the secondary coil.

In Figure 2, the lumped structure of a WPT system with a SS compensation topology is given. The DC supply voltage is converted into a high frequency square waveform by an inverter. A current flow through the primary coil and creates a time-varying magnetic field around it. Due to this magnetic field a voltage is induced in the secondary coil which is then converted to DC by a rectifier.

Table 1 lists the basic equations that should be utilized in design procedure of WPT systems with SS compensation. These equations have been used in a MATLAB (MathWorks, Inc., Natick, MA, USA) code to apply the design optimization proposed in [30].

In Table 1, V1 $\mathbb{R}_L$ and $\mathbb{R}_1$-$\mathbb{R}_2$ represent the resonant frequency, input voltage, load resistance, primary and secondary coil resistances and quality factor of secondary, respectively.

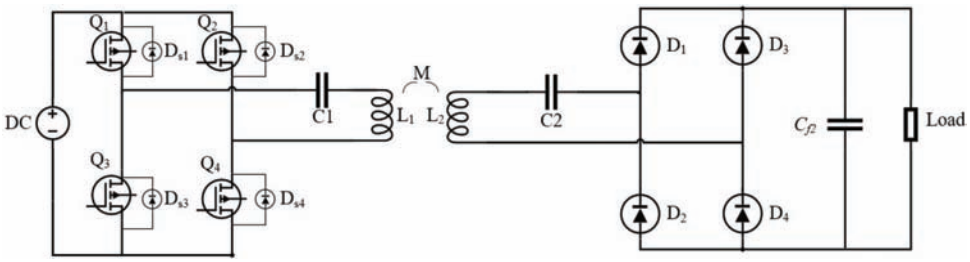

Figure 2. Lumped structure of a WPT system.

Table 1. Equations for WPT system with SS compensation[30].

Parameter	Equation
Primary side current	$I_1 = \frac{V_1}{Z_T}$
Secondary side current	$I_2 = \frac{j\omega_0 M I_1}{R_2+R_L+j(L_2\omega_0-\frac{1}{C_2\omega_0})}$
Primary compensation capacitor	$C_1 = \frac{1}{\omega_0 L_1}$
Secondary compensation capacitor	$C_2 = \frac{1}{\omega_0 L_2}$
Equivalent impedance	$Z_T = (R_1 + j(L_1\omega_0 - \frac{1}{C_1\omega_0})) + \frac{\omega_0^2 M^2}{R_2+R_L+j(L_2\omega_0-\frac{1}{C_2\omega_0})}$
Primary side quality factor	$Q_1 = \frac{L_1 R_L}{\omega_0 M^2}$
Secondary quality factor	$Q_2 = \frac{\omega_0 L_2}{R_L}$
Power transferred to load	$P_T = \frac{\omega_0 M^2 Q_2 I_1^2}{L_2}$

3. Proposed coil design and inductance calculation for hexagonal coils

In this part of the work, first of all the inductance calculation procedure and steps are given briefly. A fast and accurate calculation method is used, which is given in detail in [38]. By using the inductance equations obtained an optimal design of a 1-kW WPT system with the hexagonal coil is presented. Inductance calculations of hexagonal coils require solution of complex integrals obtained by using the Biot Savart law. However, this process can be simplified by using some approximations such as dividing the inner area of the coil into rectangular and triangular pieces [25, 34]. The total flux in the inner area of the coil can be obtained by summing these flux values. However, complex integration steps exist for the triangular areas, and several integration coefficients must be used. The approximation used in this paper is to divide the triangular areas into smaller rectangular pieces as shown in Figure 3. Then, simple magnetic flux equations based on the Biot Savart law are solved for each small region to calculate the flux density. By using (3) the magnetic flux density for each area can be calculated.

$$\overrightarrow{B_1} = \frac{u_0 I_1}{4\pi} \frac{(y_1 - 2k\sqrt{3})}{[(y_1 - 2k\sqrt{3})^2 + z_1^2]} [\frac{x_1 + 2k}{\sqrt{((x_1 + 2k)^2 + (y_1 - 4k\sqrt{3})^2 + z_1^2)}} - \frac{-x_1 + 2k}{\sqrt{((x_1 - 2k)^2 + (y_1 - 2k\sqrt{3})^2 + z_1^2)}}]\widehat{k} \quad (3)$$

where u_0 is the magnetic permeability of air and B_1 is the magnetic flux density at any P (x_1, y_1, z_1) point in the inner area of the secondary coil created by the current (I_1) passing through the primary coil.

In Figure 3, 2k and 2m show the side lengths of the single turn primary and secondary coils respectively. In order to calculate an accurate inductance value for multi-turn spiral coils, an average side length $(2k_{avg})$

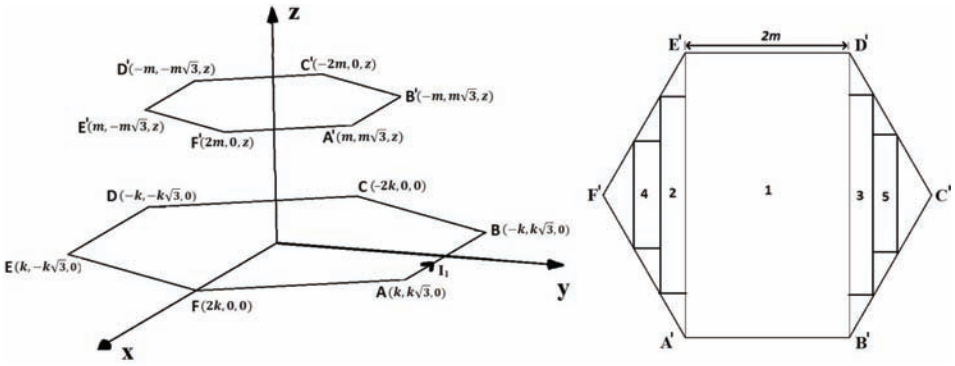

Figure 3. (a) Presentation of single turn hexagonal coils on specified coordinates, (b) Subdividing the inner area of hexagonal coil into pieces.

should be used. The average value ($2k_{avg}$) of the outer ($2k_{out}$) and inner ($2k_{in}$) side lengths for both coils can be obtained by using simple trigonometric equations. In (4), the formula for calculating the average side length of a multi-turn primary coil is given.

$$2k_{avg} = \frac{2k_{out} - [N\mathbf{w} + (N-1)g]}{2\sqrt{3}} \tag{4}$$

where w, g and N show the turn width, turn spacing and number of turns, respectively.

Integration of (3) over the surface area of individual regions yield the corresponding flux values. Then, summing these flux values will give the total flux. At the first step of sectoring the area enclosed by a coil, the largest rectangular area in the middle is created. Then, both sides of this region is divided into smaller rectangles in a symmetrical fashion yielding, for example, identical regions of 2-3 in one side and 4-5 in the other side. As the division process goes on and more and more rectangular pieces are created, the triangular regions that remain at the edges become very small and can be neglected. An iteration process is applied in order to obtain an accurate inductance value by finding the optimum number of rectangular sub-areas in the main triangle areas AEF and BCD. An algorithm used to find an accurate inductance calculation is given in [38]. The iteration process continues until the change between two obtained inductance values is reduced to 0.001%. The algorithm stops the division of the regions if the determined change is reached since the calculated value is accepted as accurate and taken as the final inductance value. The height of the formed isosceles triangle is divided into n identical parts. Let the number of rectangular regions be i. Thus, the sum of the calculated flux in the rectangular pieces from i to n-i gives the total flux of the equivalent triangular region. Equation (5) shows the flux calculation and integral boundaries for small rectangular pieces obtained by dividing the triangular regions.

$$\varphi = \frac{u_0 I}{4\pi} \int_{-m\sqrt{3}(\frac{n-i}{n})}^{m\sqrt{3}(\frac{n-i}{n})} \int_{m(\frac{n+i-1}{n})}^{m(\frac{n+i}{n})} \frac{(k\sqrt{3}-y_1)}{[(k\sqrt{3}-y_1)^2+z_1^2]} \left[\frac{k+x_1}{\sqrt{((k+x_1)^2+(k\sqrt{3}-y_1)^2+z_1^2)}} + \frac{k-x_1}{\sqrt{((k-x_1)^2+(k\sqrt{3}-y_1)^2+z_1^2)}} \right] dx_1 dy_1 \tag{5}$$

3.1. Mutual inductance

The mutual inductance between two hexagonal coils can be found by calculating the magnetic flux in the inner area of the secondary coil generated by the current flowing through one side length (AB) of the primary coil. The sum of the fluxes of large rectangle and identical triangle areas gives the flux value for the inner area of the secondary coil generated by the segment AB and it is given in (6). φ_{AB,Δ_1} ,φ_{AB,Δ_2} and $\varphi_{AB,\mathbb{R}_1}$ show the flux for the first and second triangle areas and large rectangular area, respectively. Thus, the total amount of flux (φ_{Total}) will be six times the value of flux obtained with a side length and it is given in (7).

$$\varphi = (\varphi_{AB,\Delta_1} + \varphi_{AB,\Delta_2} + \varphi_{AB,\mathbb{R}_1}) \tag{6}$$

$$\varphi_{Total} = 6\varphi_{AB} \tag{7}$$

After this solution process, the mutual inductance formula can be obtained as

$$M = N_1 N_2 \frac{\varphi_{Total}}{I} \tag{8}$$

3.2. Self-inductance

Self-inductance calculation of a hexagonal coil structure can be obtained with a similar method. By the integration of the magnetic flux density of an arbitrary point in the inner area of hexagonal coil through the surface enclosed by the side edges of the coil, the total flux value can be obtained. The main flux density formula and the integration with the boundaries are given in cylindrical coordinate system in (9) and (10), respectively.

$$\overrightarrow{B} = \frac{u_0 I}{4\pi r}[\frac{z+k}{\sqrt{(z+k)^2+r^2}} - \frac{z-k}{\sqrt{(z-k)^2+r^2}}]\widehat{\varphi} \tag{9}$$

With the same approach of mutual inductance calculation, the total magnetic flux in the two identical triangles and a large rectangular area is calculated to obtain the self-inductance value by dividing the triangle areas into rectangular pieces. The same iteration process has been done for obtaining an accurate value of the self-inductance. The magnetic flux equation for the triangle areas, which are divided into rectangular areas, depends on the side length of the hexagon and the division parameters n and i as given in (10).

$$\begin{aligned} \varphi_{AB} &= \frac{u_0 I}{4\pi} \int_{(\frac{k\sqrt{3}i}{n})}^{k\sqrt{3}(\frac{2n-i}{n})} \int_{k(\frac{n+i-1}{n})}^{k(\frac{n+i-1}{n})} B dz dr \\ &= \frac{u_0 I}{4\pi} \int_{(\frac{k\sqrt{3}i}{n})}^{k\sqrt{3}(\frac{2n-i}{n})} \int_{k(\frac{n+i-1}{n})}^{k(\frac{n+i-1}{n})} \left[\frac{z+k}{\sqrt{(z+k)^2+r^2}} - \frac{z-k}{\sqrt{(z-k)^2+r^2}}\right] dz dr \end{aligned} \tag{10}$$

Similar flux equations are derived for the rectangular and the triangle areas to obtain total fluxes. After derivation, they are summed up and the total flux equation is obtained as given below.

$$\varphi_{AB,total} = 6(\varphi_{T,AB,\Delta} + \varphi_{AB,rectangular}) \tag{11}$$

As a result, the self-inductance formula of a hexagonal coil for any size and coil radius can be simplify as

$$L_{hexagon} = \frac{6N^2(2\varphi_{AB,\Delta} + \varphi_{AB,rectangular})}{I} \tag{12}$$

The equations given in Table 1 and the inductance equations given above are used in the optimization algorithm to obtain optimum the parameters of the 1 kW WPT system design with a 10 cm air gap between the primary and secondary coils. The main design parameters are listed in Table 2.

Table 2. Design parameters.

Parameter	Calculated value
$C_1(nF)$	411.92
$C_2(nF)$	460.97
$L_1(\mu H)$	155.82
$L_2(\mu H)$	139.24
M(μH)	29.73
N_1	10
N_2	11
f(kHz)	19.86

The design process yields 10 turns with 2.58 mm^2 wire cross section area and 310 mm side length (k_{out}) for the primary coil and 11 turns with 2.48 mm^2 wire cross section and 248 mm side length (m_{out}) for the secondary coil. A 3D model of the coils with these specifications is created by the FEA based ANSYS Maxwell software. The coils were also manufactured in the laboratory as shown in Fig. 4. Litz wires with a cross section of 2.5 mm^2 were used for both coils. The inductance values obtained by the numerical method used in this work, the FEA simulation and the measurements by an LCR meter are listed in Table 3.

Figure 4. Manufactured coils and 3D FEA Model

As can be seen in Table 2, the obtained numerical, FEA and measured values are well matching. The calculated self-inductance value of the primary coil has 5.6 % percent error if compared to measured results where the calculated value of the secondary coil has an 5 % percent error. Furthermore, the mutual inductance is well matching with an 5.8 % percent error when compared to measured results.

Table 3. Comparison of the inductance results.

Method	Self Inductance (μH)		Mutual inductance(μH)
	Primary coil	Secondary coil	
Measured	147.48	132.51	31.57
FEA	145.62	127.82	30.09
Numerical	155.82	139.24	29.73
Error(%)	5.6	5	5.8

4. Simulation and experimental results

This section presents the results of the simulation and experimental results of the 1-kW system designed in the previous section. The magnetic parts of the system were simulated in ANSYS Maxwell while the rest was simulated in Simplorer simultaneously. The system model is shown in Figure 5.

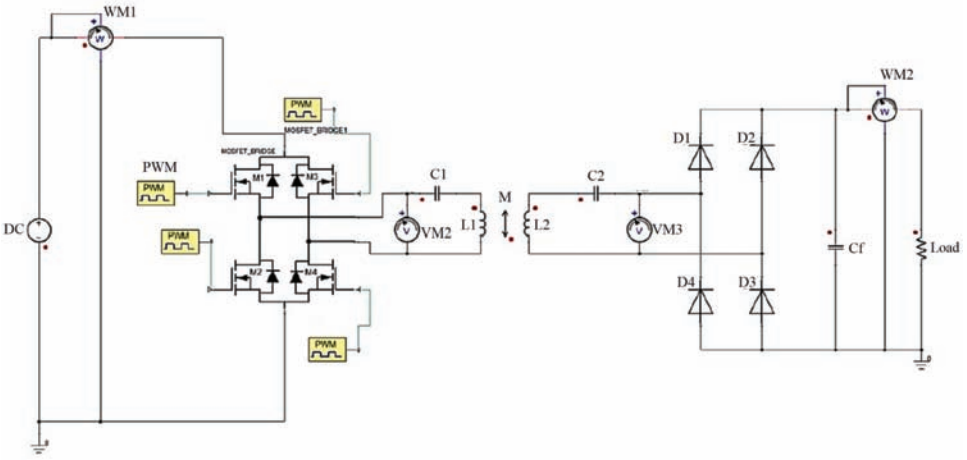

Figure 5. Simulation model of designed WPT system

A 72 V DC source is feeding the system and this voltage is converted to a high frequency square voltage wave form by full bridge inverter. A pure resistive load (R_{dc}) is connected to the output of the circuit. The equivalent AC resistor seen by the compensation circuit is found by using the fact that the average power values on both sides of the ideal bridge are equal. This yields $R_{ac} = R_{dc}\ \pi^2/8 = 1.23\ R_{dc}$. This would give an equivalent load resistance 4.56 Ω. The values given in Table 2 have been found by using this resistance. The primary and secondary side current and voltage wave forms are presented in Fig. 6.

The efficiency of coil to coil can be calculated from the obtained wave forms. The power calculated on the primary side is 1122 W and the power calculated on the secondary side is 1028 W. The efficiency is calculated as 91.6 %. When the simulation results are considered, it can be concluded that expected results can be obtained and system performance can be observed with these parameters in the laboratory with an experimental setup. For this purpose, the manufactured coils and power electronic circuit were combined and the system was realized. The experimental setup is shown in Figure 7.

A DC power supply is used to feed the full bridge inverter. IGBT's are used to produce high frequency square wave form. Resonance capacitors values, which are closest to the capacitor values given in Table 2 and

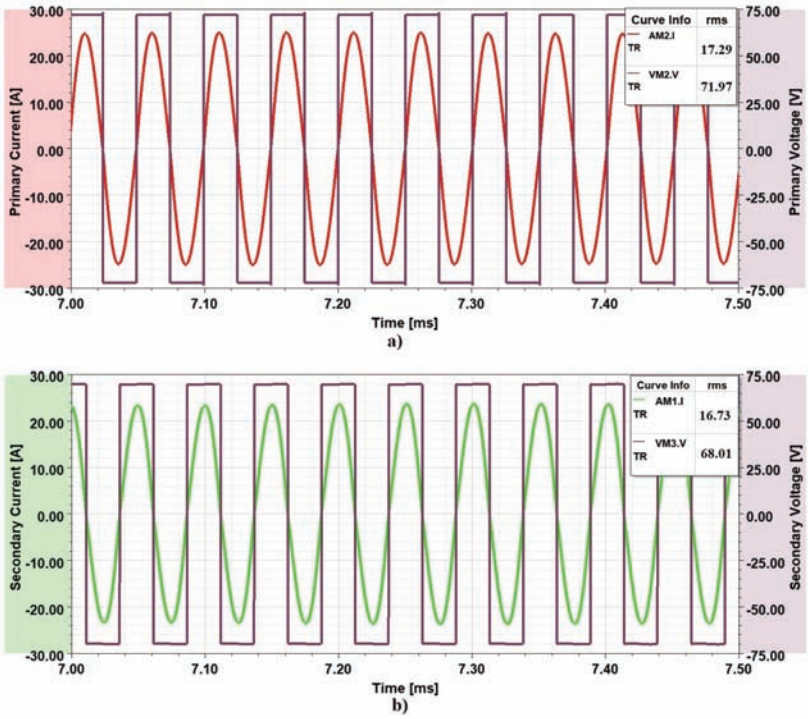

Figure 6. Simulation results. a) Primary side current and voltage waveforms, b) Secondary side current and voltage waveforms.

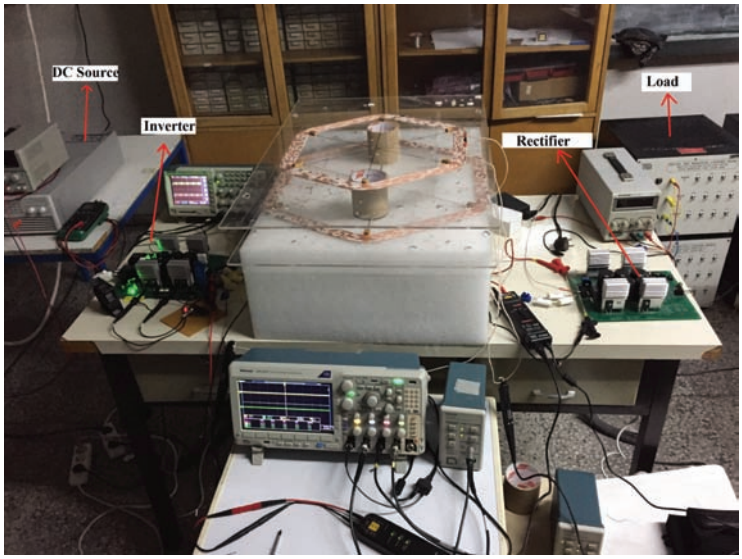

Figure 7. Experimental setup with the manufactured coils and power electronic circuit.

available under laboratory conditions, were measured for the primary and secondary side with an LCR meter as $C_1 = 415$ nF and $C_2 = 475$ nF, respectively. In order to get the highest resonance state with these parameters the resonance frequency varied as it is possible to get the best. At 19.9 kHz with a slight phase difference between the current and voltage waveforms can be obtained and the measurement results are taken with this operating frequency.

In Figure 8 the measurement results of the primary and secondary side current and voltage wave forms are given respectively. As it can be seen, the measurement results are well matched with simulation results and the design is verified. The input power, current and voltage values recorded from DC power supply. The out power on the load is calculated by the current and voltage rms values recorded with the current probe and multimeter. These recorded values are given in Table 4 and the current and voltage values are in RMS. The efficiency of the system from end to end can be calculated as 85% which shows a highly efficient WPT system is designed and implemented even with a large air gap of 10 cm between the primary and secondary coils. Switching losses, losses due to phase shifting on the primary side and copper losses due to winding resistance constitute the losses of the circuit.

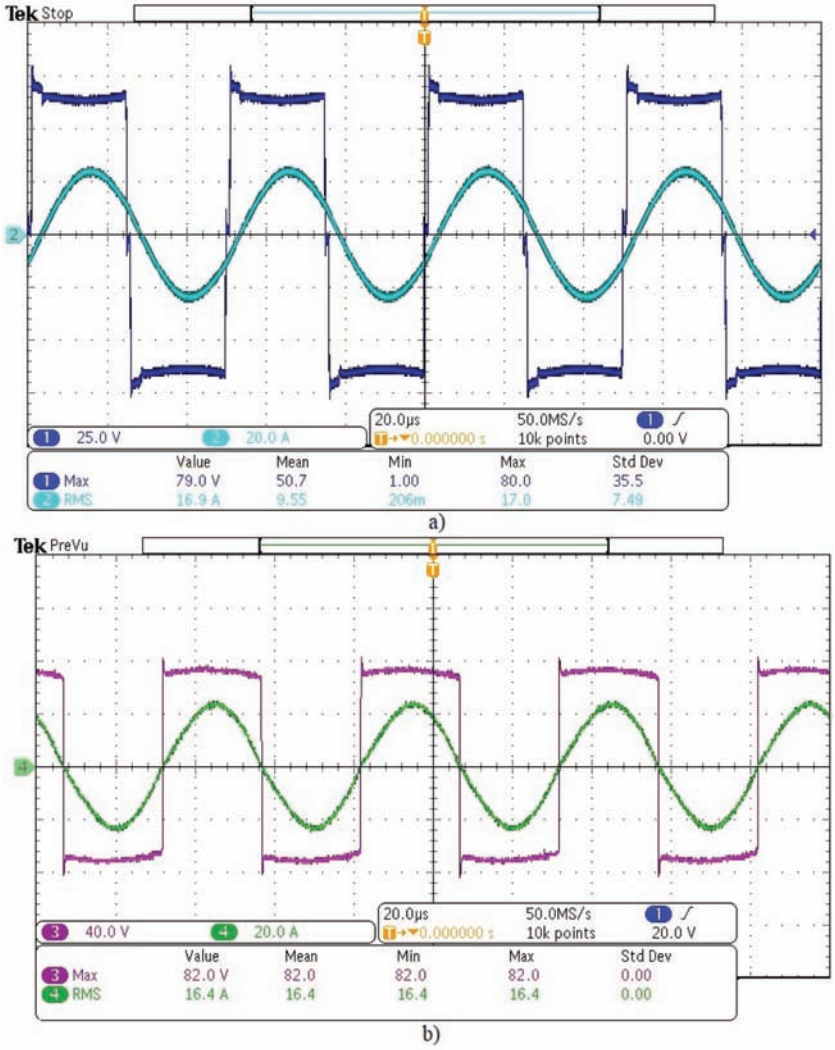

Figure 8. Measured a) Primary side current and voltage waveforms, b) Secondary side current and voltage waveforms.

In order to see the variation of the output power according to the misalignment between the coils on the x and y axes, the secondary winding was shifted 80, 160 and 240 mm on both the x and y axes, respectively. Measurement results for the variation of the output power against to different positioning of the secondary coil is given in Figure 9.

Table 4. Measured voltage, current and power values

	Voltage(V)	Current (A)	Power (W)
Input	72	15.8	1137
Output	63.2	15.3	967

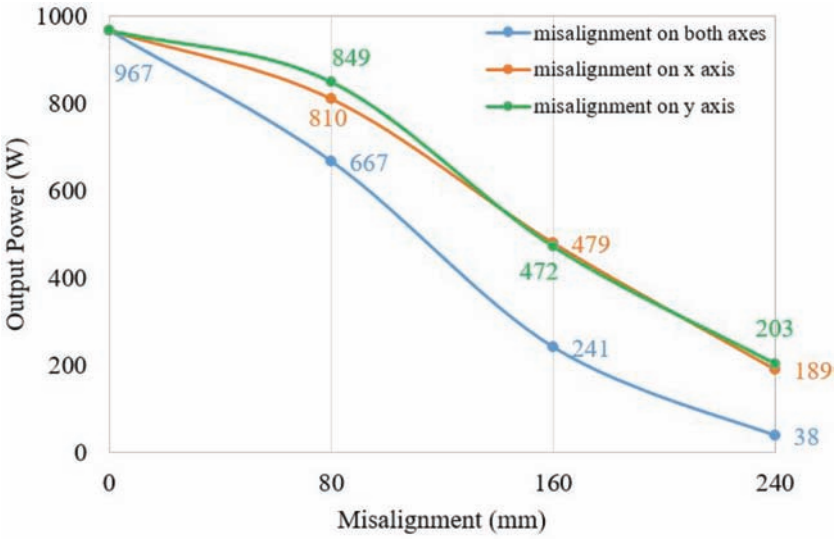

Figure 9. Variation of output power against to misalignment.

Shifting the secondary coil on x or y axes the effect of misalignment on the output power is approximately the same. But it can be seen that the output power almost approaches zero in case of 240 mm shifting the secondary coil on both axes, which is the worst case and it is not a situation in real practice. Especially in SS topology, a closed loop control system must be integrated to the setup since in some cases the output power almost become zero. As a result, 85% efficiency value obtained in perfect alignment without using cores can be evaluated as an important achievement. To comply the design with international health standards an aluminum shielding added and an eddy current simulation was done on ANSYS Maxwell software. An aluminum sheet with 430 × 500 mm dimensions is used as the shielding and is placed on the secondary coil as given in Figure 10.

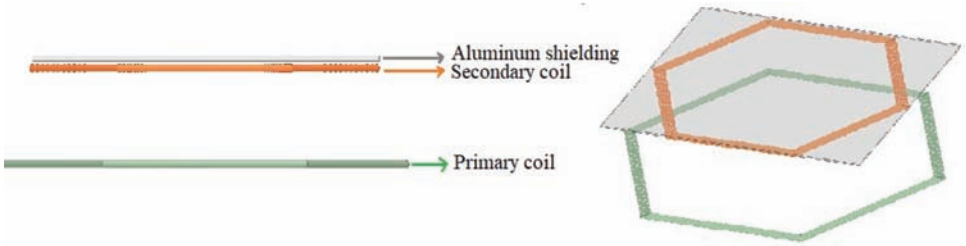

Figure 10. Shielding added design

The reference points for measuring flux density values are determined with considering a sedan EV car dimensions. The magnetic flux density B (μT) values were obtained from the secondary coil at the distance of

300, 520, 870, 1220, 1570 and 1670 mm, respectively. The reference points and obtained flux density values are given in Figure 11.

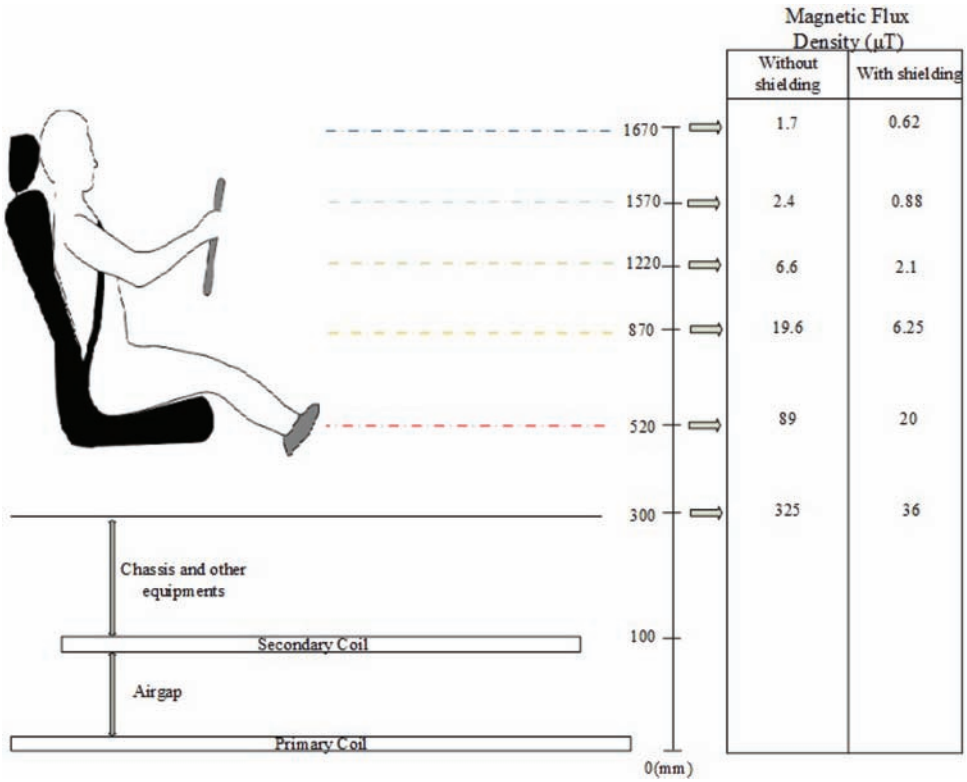

Figure 11. Magnetic flux density exposure values for a driver.

When the simulation results obtained are analyzed, it is seen that the use of shielding greatly reduces the magnetic field value exposed. According to the ICNIRP standard, the magnetic flux density exposed should not exceed 6.25 μT and should not exceed $\sqrt{20}$ times this value, i.e. 27.3 μT. In the analysis made without using screening, it is seen that the flux density values obtained at the foot and lower points in the human model given in Figure 11 are above of this threshold value. With the use of shielding to eliminate this negative situation, it can be seen that all values from the first part of the human body to the beginning, are below the allowable threshold values and a successful shielding can be done. As a result of the analysis made using screening, the highest value that the human body is exposed to in Fig. 11 is 20 μT, which is an allowed value while the magnetic flux density value in the head section is only 0.62 μT.

5. Conclusion

In this study, a 1 kW WPT system design with a hexagonal coil is proposed and implemented. Calculating the inductance values accurately is a critical issue to obtain optimum design parameters for the target power. From this view, the mutual and self-inductance equations are obtained and the results show that the calculated inductance values well match with the FEA model and measurement results. By using the inductance equations, a S-S compensated WPT system was designed at 1 kW power and the performance of the system was evaluated by using ANSYS software. In order to verify the analytical and simulation results, the coils are manufactured with respecting the optimum specifications and the system is implemented in the laboratory. The measurement

results are well matched with the analytical and simulation results and 85 % power efficiency is achieved from end to end system. In addition, to comply the design with international health standards an aluminum shielding placed on the secondary coil and the effect of the shielding on the magnetic field results is obtained by simulation. The maximum magnetic field density value is obtained as 20 µT, which is an acceptable value according to the international standards. This study shows that using a single primary and secondary coils supports the idea of transferring power wirelessly is possible even without using core material and indicates that WPT system with a hexagonal coil is preferable for charging the EV's batteries. For the future work, the hexagonal coil arrays can be used for better coupling and misalignment tolerance for stationary and dynamic charging of EV's with higher power values.

Acknowledgment

This work was supported by Scientific and Technological Research Council of Turkey (TUBITAK) with the project contract 5160042. Authors would like thank to TUBITAK and the project team for this support. We would also like thank to Mr. Yusuf Kosesoy for his support in the experimental work.

References

[1] Villa JL, Lombart A, Sanz JF, Sallan J. Practical Development of a 5 kW ICPT System SS Compensated with a Large Air gap. In: IEEE International Symposium on Industrial Electronics, Vigo; 2007. pp. 1219-1223.

[2] Jang Y, Jovanovic M. A contactless electrical energy transmission system for portable-telephone battery chargers. IEEE Transactions on Industrial Electronics 2003; 50 (3): 520-527.

[3] Ram Rakhyani AK, Mirabbasi S, Chiao M. Design and Optimization of Resonance-Based Efficient Wireless Power Delivery Systems for Biomedical Implants. IEEE Transactions on Biomedical Circuits and Systems 2011; 5 (1) pp. 48-63.

[4] Ma H, Yang Y, Qi N, Ma S, Li X. Demonstration of a high-efficiency MWPT System for Aerospace. In: IEEE Wireless Power Transfer Conference (WPTC), Montreal, QC, Canada; 2018. pp. 1-4.

[5] Zhu D, Grabham NJ, Clare L, Stark BH, Beeby SP. Inductive power transfer in e-textile applications: Reducing the effects of coil misalignment. In: IEEE Wireless Power Transfer Conference (WPTC), Boulder, CO; 2015. pp. 1-4.

[6] Kylee DS, Efe V, Susan M, PattersonRyan J, BohmMorris PK. Wireless power transfer for a seat-vest-helmet system. US Patent, US20150115733A1, Witricity Co., 2015.

[7] Peter KJ, Elangovan D, Arunkumar G. Linear control of wireless charging for electric bicycles. Applied Energy 2019; vol.255.

[8] Hutin M, Leblanc M. Transformer system for electric railways. US patent 527 857, Oct. 23, 1894.

[9] Abel E, Third S. Contactless power transfer–An exercise in topology. IEEE Transactions on Magnetics 1984; 20 (5): 1813-1815.

[10] Delmas A, Omeich M, Rioux C. High efficiency inductive energy transfer. In: 7th Pulsed Power Conference, Monterey, CA, USA; 1989. pp. 598-601.

[11] Kurs A, Karalis A, Moffatt R, Joannopoulos JD, Fisher P et al. Wireless Power Transfer via Strongly Coupled Magnetic Resonances. Science 2007; 317, 83-86.

[12] Ahmed AS, Mohamed Ahmed A, Shaier HM, Sameh IS. A comprehensive overview of inductive pad in electric vehicles stationary charging. Applied Energy 2020; Volume 262.

[13] Budhia M, Boys JT, Covic GA, Chang-Yu H. Development of a Single-Sided Flux Magnetic Coupler for Electric Vehicle IPT Charging Systems. IEEE Transactions on Industrial Electronics 2013; 60 (1): 318-328.

[14] Ahn D, Hong S. A Study on Magnetic Field Repeater in Wireless Power Transfer. IEEE Transactions on Industrial Electronics 2013; 60 (1): 360-371.

[15] Kim J, Son H, Kim K, Park Y. Efficiency Analysis of Magnetic Resonance Wireless Power Transfer With Intermediate Resonant Coil. IEEE Antennas and Wireless Propagation Letters 2011;, vol. 10: 389-392.

[16] Lee CK, Zhong WX, Hui SYR. Effects of Magnetic Coupling of Nonadjacent Resonators on Wireless Power Domino-Resonator Systems. IEEE Transactions on Power Electronics 2012; 7 (4): 1905-1916.

[17] Nagendra GR, Covic, GA, Boys JT. Determining the Physical Size of Inductive Couplers for IPT EV Systems. IEEE Journal of Emerging and Selected Topics in Power Electronics 2014; 2 (3): 571-583.

[18] Lin FY, Zaheer A, Budhia M, Covic GA. Reducing leakage flux in IPT systems by modifying pad ferrite structures. In: IEEE Energy Conversion Congress and Exposition (ECCE), Pittsburgh, PA; 2014. pp. 1770-1777.

[19] Kalwar K, Mekhilef S, Seyedmahmoudian M, Horan B. Coil Design for High Misalignment Tolerant Inductive Power Transfer System for EV Charging. Energies 2016; 9 (11) :937.

[20] Lin F, Covic GA, Boys JT. A Comparison of Multi-Coil Pads in IPT systems for EV Charging. In: IEEE Energy Conversion Congress and Exposition (ECCE), Portland, OR; 2018. pp. 105-112.

[21] Sis Seyit A, Orta Emre. A Cross-Shape Coil Structure for Use in Wireless Power Applications. Energies 2018; 11 (5): 1094.

[22] Sis Seyit A, Kılıç F, Sezen S. Multi sub-coil flux pipe couplers and their use in a misalignment-adaptive wireless power transfer system. Journal of Electromagnetic Waves and Applications 2019; 33(14).

[23] Pearce MGS, Covic GA, Boys JT. Robust Ferrite-Less Double D Topology for Roadway IPT Applications. IEEE Transactions on Power Electronics 2019; 34 (7): 6062-6075.

[24] Aydin E, Kosesoy Y, Yildiriz E, Aydemir MT. Comparison of Hexagonal and Square Coils for Use in Wireless Charging of Electric Vehicle Battery. In: IEEE International Symposium on Electronics and Telecommunications (ISETC), Timisoara, Romania;2018.

[25] Tan P, Yi F, Liu C, Guo, Y. Modeling of Mutual Inductance for Hexagonal Coils with Horizontal Misalignment in Wireless Power Transfer. In: IEEE Energy Conversion Congress and Exposition (ECCE), Portland, OR, USA; 2018.

[26] Junjun D, Bo P, Wenli S, Zhenpo W. A new integration method with minimized extra coupling effects using inductor and capacitor series-parallel compensation for wireless EV charger. Applied Energy 2017; vol. 207: 405-416.

[27] Houran AM, Yang X, Chen W. Magnetically Coupled Resonance WPT: Review of Compensation Topologies, Resonator Structures with Misalignment, and EMI Diagnostics. Electronics 2018; 11 (22).

[28] Shevchenko V, Husev O, Strzelecki R, Pakhaliuk B, Poliakov N et al. Compensation Topologies in IPT Systems: Standards, Requirements, Classification, Analysis, Comparison and Application. IEEE Access 2019; vol. 7: 120559-120580.

[29] Jiang C, Chau KT, Liu C, Lee CHT. An Overview of Resonant Circuits for Wireless Power Transfer. Energies 2017; 10 (7):894.

[30] Sallan J, Villa JL, Llombart A, ve Sanz JF. Optimal design of ICPT systems applied to electric vehicle battery charge. IEEE Transaction on Industrial Electronics 2009; 56 (6): 2140-2149.

[31] Barmada S, Fontana N, Tucci M. Design Guidelines for Magnetically Coupled Resonant Coils with Data Transfer Capability. In: International Applied Computational Electromagnetics Society Symposium (ACES), Miami, FL, USA; 2019. pp. 1-2.

[32] Mohan SS, Mar Hershenson M, Boyd SP, Lee TH. Simple accurate expressions for planar spiral inductances. IEEE Journal of Solid-State Circuits 1999; 34 (10): 1419-1424.

[33] Grover FW. Formulas and tables for the calculation of the inductance of coils of polygonal form. Scientific Papers of the Bureau of Standards 1922; vol. 18: 737-762.

[34] Tavakkoli H, Ebrahim AS, Amin K, Ghader R, Khoei A. Analytical study of mutual inductance of hexagonal and octagonal spiral planer coils. Sensors & Actuators A Physical 2016; vol. 247: 53-64.

[35] Tran DH, Vu VB, Choi W. Design of a High-Efficiency Wireless Power Transfer System with Intermediate Coils for the On-Board Chargers of Electric Vehicles. IEEE Transactions on Power Electronics 2018; 33 (1): 175-187.

[36] ICNIRP Guidelines, For limiting exposure to time-varying electric and magnetic fields (1 Hz–100 kHz). Health Physics 2010; 99 (6): 818–836.

[37] Boys JT, Covic GA, Green AW. Stability and control of inductively coupled power transfer systems. IEE Proceedings - Electric Power Applications 2000; 147 (1): 37-43.

[38] Aydin E, Yildiriz E, Aydemir MT. A new semi-analytical approach for self and mutual inductance calculation of hexagonal spiral coil used in wireless power transfer systems. Electrical Engineering 2021.